Nonlinear optical coefficients and phase-matching conditions in $Sn_2P_2S_6$

D. Haertle, M. Jazbinšek, G. Montemezzani*, P. Günter

Nonlinear Optics Laboratory, Institute of Quantum Electronics, Swiss Federal Institute of Technology, ETH Hönggerberg, CH-8093 Zürich (Switzerland)

* *Present address: Laboratoire Matériaux Optiques, Photonique et Systèmes (LMOPS, UMR CNRS 7132), Université de Metz et Supélec, 2 rue E. Belin, F - 57070 Metz Cedex*

dhaertle@phys.ethz.ch

http://www.nlo.ethz.ch

Abstract: Phase matching conditions and second and third order nonlinear optical coefficients of $Sn_2P_2S_6$ crystals are reported. The coefficients for second harmonic generation (SHG) are given at $\lambda = 1542$ nm and 1907 nm at room temperature. The largest coefficients at these wavelengths are $d_{111} = 17 \pm 1.5\,\mathrm{pm/V}$ and $d_{111} = 12 \pm 1.5\,\mathrm{pm/V}$, respectively. The third-order subsceptibilities $\chi^{(3)}_{1111} = (17 \pm 6) \cdot 10^{-20}\,\mathrm{m^2/V^2}$ and $\chi^{(3)}_{2222} = (9 \pm 3) \cdot 10^{-20}\,\mathrm{m^2/V^2}$ were determined at $\lambda = 1907$ nm. All measurements were performed by the Maker-Fringe technique. Based on the recently determined refractive indices, we analyze the phase-matching conditions for second harmonic generation, sum- and difference-frequency generation and parametric oscillation at room temperature. Phase-matching curves as a function of wavelength and propagation direction are given. Experimental phase-matched type I SHG at 1907 nm has been demonstrated. The results agree very well with the calculations. It is shown that phase-matched optical parametrical oscillation is possible in the whole transparency range up to $8\,\mu$m with an effective nonlinear coefficient $d_{\mathrm{eff}} \approx 4\,\mathrm{pm/V}$.

OCIS codes: (160.4330) Nonlinear optical materials; (190.2620) Frequency conversion

References and links

1. S. G. Odoulov, A. N. Shumelyuk, U. Hellwig, R. A. Rupp, A. A. Grabar, and I. M. Stoyka, "Photorefraction in tin hypothiodiphosphate in the near infrared," J. Opt. Soc. Am. B **13**, 2352–60 (1996).
2. M. Jazbinsek, G. Montemezzani, P. Gunter, A. A. Grabar, I. M. Stoika, and Y. M. Vysochanskii, "Fast near-infrared self-pumped phase conjugation with photorefractive $Sn_2P_2S_6$," J. Opt. Soc. Am. B. June **20**, 1241–6 (2003).
3. D. Haertle, G. Caimi, A. Haldi, G. Montemezzani, P. Günter, A. A. Grabar, I. M. Stoika, and Y. M. Vysochanskii, "Electro-optical properties of $Sn_2P_2S_6$," Opt. Commun. **215**, 333–43 (2003).
4. M. I. Gurzan, A. P. Buturlakin, V. S. Gerasimenko, N. F. Korde, and V. Y. Slivka, "Optical properties of $Sn_2P_2S_6$ crystals," Soviet Physics Solid State **19**, 1794–5 (1977).
5. A. Anema, A. Grabar, and T. Rasing, "The nonlinear optical properties of $Sn_2P_2S_6$," Ferroelectrics **183**, 181–3 (1996).
6. D. Haertle, A. Guarino, J. Hajfler, G. Montemezzani, and P. Günter, "Refractive indices of $Sn_2P_2S_6$ at visible and infrared wavelengths," Opt. Express **13**, 2047–57 (2005).
7. G. Dittmar and H. Schäfer, "Die Struktur des Di-Zinn-Hexathiohypo-diphosphats $Sn_2P_2S_6$," Zeitschrift fuer Naturforschung **29B**, 312–7 (1974).

#7179 - $15.00 US
Received 15 April 2005; revised 3 May 2005; accepted 5 May 2005

8. F. Brehat and B. Wyncke, "Calculation of double-refraction walk-off angle along the phase-matching directions in non-linear biaxial crystals," J. Phys. B **22**, 1891–8 (1989).
9. B. Wyncke and F. Brehat, "Calculation of the effective second-order non-linear coefficients along the phase matching directions in acentric orthorhombic biaxial crystals," J. Phys. B **22**, 363–76 (1989).
10. J. Q. Yao and T. S. Fahlen, "Calculations of optimum phase match parameters for the biaxial crystal $KTiOPO_4$," J. Appl. Phys. **55**, 65–8 (1984).
11. R. C. Miller, "Optical 2nd harmonic generation in piezoelectric crystals," Appl. Phys. Lett. **5**, 17–9 (1964).
12. W. J. Alford and A. V. Smith, "Wavelength variation of the second-order nonlinear coefficients of $KNbO_3$, $KTiOPO_4$, $KTiOAsO_4$, $LiNbO_3$, $LiIO_3$, beta -BaB_2O_4, KH_2PO_4, and LiB_3O_5 crystals: a test of Miller wavelength scaling," J. Opt. Soc. Am. B **18**, 524–33 (2001).
13. D. A. Roberts, "Simplified characterization of uniaxial and biaxial nonlinear optical crystals: a plea for standardization of nomenclature and conventions," IEEE Journal of Quantum Electronics **28**, 2057–74 (1992).
14. J. Jerphagnon and S. K. Kurtz, "Maker fringes: a detailed comparison of theory and experiment for isotropic and uniaxial crystals," J. Appl. Phys. **41**, 1667–81 (1970).
15. C. Bosshard, U. Gubler, P. Kaatz, W. Mazerant, and U. Meier, "Non-phase-matched optical third-harmonic generation in noncentrosymmetric media: Cascaded second-order contributions for the calibration of third-order nonlinearities," Phys. Rev. B **61**, 10,688–701 (2000).
16. M. Zgonik, M. Copic, and H. Arend, "Optical second harmonic generation in ferro- and para-electric phases of $PbHPO_4$," J. Phys. C **20**, L565–569 (1987).
17. R. S. Klein, G. E. Kugel, A. Maillard, K. Polgar, and A. Peter, "Absolute non-linear optical coefficients of $LiNbO_3$ for near stoichiometric crystal compositions," Opt. Mat. **22**, 171–4 (2003).
18. B. Boulanger, J. P. Feve, G. Marnier, B. Menaert, X. Cabirol, P. Villeval, and C. Bonnin, "Relative sign and absolute magnitude of $d^{(2)}$ nonlinear coefficients of KTP from second-harmonic-generation measurements," J. Opt. Soc. Am. B **11**, 750–7 (1994).

1. Introduction

Tin thiohypodiphosphate ($Sn_2P_2S_6$) is a wide bandgap semiconductor ferroelectric with very attractive photorefractive properties [1, 2] and large electro-optical coefficients [3]. In addition, the wide optical transparency range extending from $\lambda = 0.53$ μm to $\lambda = 8$ μm [4] holds promise for optical parametric generation up to infrared wavelengths not accessible with standard nonlinear optical crystals. This requires the knowledge of the nonlinear optical coefficients and phase matching conditions. Up to now no coefficient had been determined; the only publication on nonlinear optics in $Sn_2P_2S_6$ reports a value for d_{211} [5], but unfortunately without specifying the coordinate system being used (in $Sn_2P_2S_6$ d_{211} is zero due to symmetry in the standard coordinate system). In this work we determine or estimate all 10 second-order nonlinear coefficients, as well as the third-order nonlinear optical susceptibilities $\chi^{(3)}_{1111}$ and $\chi^{(3)}_{2222}$ using the Maker-Fringe technique.

In Ref. 6 the refractive indices and the indicatrix rotation of $Sn_2P_2S_6$ are given for the wavelength range $550 - 2300$ nm at room temperature. The Sellmeier coefficients determined there allow to describe the refractive indices with an accuracy of $2 \cdot 10^{-4}$ in the wavelength interval indicated. These data allow us to calculate phase-matching conditions for second harmonic generation (SHG), sum- and difference-frequency generation (SFG and DFG) and optical parametric oscillation (OPO). Calculated phase-matching conditions are compared with experimental data at $\lambda = 1907$ nm. A configuration for optical parametric oscillators pumped with the fundamental wavelength of a Nd:YAG laser, capable of producing radiation from 1 to 8 μm in the infrared with a high gain ($d_{\text{eff}} \approx 4$ pm/V), is described.

2. Optical frequency conversion in $Sn_2P_2S_6$

For phase-matched parametric interactions among three parallel waves at the frequencies ω_1, ω_2, and ω_3, where $\omega_3 = \omega_1 + \omega_2$, the vacuum wavelengths λ_i of the interacting waves must satisfy

$$\frac{n_3}{\lambda_3} = \frac{n_1}{\lambda_1} + \frac{n_2}{\lambda_2} \tag{1}$$

#7179 - $15.00 US Received 15 April 2005; revised 3 May 2005; accepted 5 May 2005

where the n_i are the refractive indices for the waves at frequencies ω_i. We use the Cartesian coordinate system as defined in Ref. 6: unit cell of Dittmar and Schäfer [7], $y \parallel b$ is perpendicular to the mirror plane of the crystal, $z \parallel c$, the positive direction of the x-axis and the z-axis so that the piezoelectric coefficients d_{xxx} and d_{zzz} are positive and $+y$ so that xyz is a right-handed system. The spherical coordinates are defined in the standard way used in physics, with θ the angle between $\mathbf{k}$ and z, and ϕ the counterclockwise angle from x to the projection of $\mathbf{k}$ to the xy-plane.

Phase-matching conditions may be satisfied in materials with sufficient birefringence either by rotating the direction of the laser beams with respect to the main axes of the optical indicatrix (angle tuning), by adjusting the wavelengths of the interacting beams (wavelength tuning), or by temperature tuning of the birefringence of the crystal.

The advantage of wavelength and temperature tuning is that the interacting beams can travel collinearly with one of the main axes of the optical indicatrix. In this case, termed noncritical phase matching, the Poynting vectors of all the interacting waves are parallel to the wave vector: The interacting beams do not walk off from one another.

For angle tuning, there is critical phase matching: The Poynting vectors are in general not parallel to the wave vectors, and the interacting beams walk off from one another [8]. The efficiency of the frequency conversion depends on the interaction length of the waves in the crystal, which in turn depends on the diameter of the beams and on the walk-off angle. Angle tuning is advantageous if the interaction length is of the order of the crystal length; the method can find application for powerful pulsed lasers when the beams do not need to be tightly focused or a long crystal length is not required.

The induced nonlinear-optical polarization $\mathbf{P}^{(\omega_3)}$ as a function of the electric fields $\mathbf{E}(\omega_{1,2})$ of the fundamental waves is described by

$$P_i^{(\omega_3)} = \varepsilon_0 \sum_{jk} d_{ijk}^{(\omega_3,\omega_1,\omega_2)} E_j^{(\omega_1)} E_k^{(\omega_2)}, \tag{2}$$

where ε_0 is electric constant and d_{ijk} are the nonlinear-optical coefficients. For second harmonic generation ($\omega_1 = \omega_2$), d_{ijk} is symmetric in the last two indices, and the contracted notation can be used.

For general directions of the wave vectors and polarizations in the crystal the projection of the induced polarization at frequency ω_3 along the direction of polarization of the emitted wave with frequency ω_3 can be written as

$$|P^{(\omega_3)}| = 2\varepsilon_0 d_{\text{eff}} |E^{(\omega_1)}|\,|E^{(\omega_2)}| \tag{3}$$

with

$$d_{\text{eff}} = \sum_{ijk} d_{ijk}^{(\omega_3,\omega_1,\omega_2)} \cos(\beta_i^{(\omega_3)}) \cos(\beta_j^{(\omega_1)}) \cos(\beta_k^{(\omega_2)}), \tag{4}$$

where $\beta_i^{(\omega)}$ is the angle between the electric-field vector of the wave at frequency ω and the axis i of the Cartesian coordinate system [9]. In a birefringent crystal the electric field direction in general is not perpendicular to the wave vector. The walk-off angle has to be taken into account in order to calculate the angles β_i [8, 10].

For type I SHG the induced nonlinear polarization is given by:

$$|P^{(2\omega)}| = \varepsilon_0 d_{\text{eff}} |E^{(\omega)}|^2, \tag{5}$$

where d_{eff} can again be derived from Eq. (4). The difference between Eqs. (5) and (3) is consistent with a continuous transition to the degenerate case, described by (5), from the sum-frequency case, described by (3), with two distinguishable fundamental fields.

#7179 - $15.00 US Received 15 April 2005; revised 3 May 2005; accepted 5 May 2005

The frequency dependence of the nonlinear-optical coefficients can be approximately described with Miller's rule [11]:

$$d_{ijk}^{(\omega_3,\omega_1,\omega_2)} = \varepsilon_0 \chi_{ii}^{(\omega_3)} \chi_{jj}^{(\omega_1)} \chi_{kk}^{(\omega_2)} \delta_{ijk}\,, \tag{6}$$

where δ_{ijk}, the Miller indices, are almost independent of the frequency [12] and $\chi_{ii} = n_i^2 - 1$ are the diagonal elements of the linear subsceptibility.

3. Second harmonic generation

In SHG the frequencies of the incoming beams are equal ($\omega_1 = \omega_2$) and the d tensor becomes symmetric in its last two indices. This allows to write it in its reduced form [13], which for the symmetry group m of $Sn_2P_2S_6$ is

$$(d_{ip}) = \begin{pmatrix} d_{11} & d_{12} & d_{13} & 0 & d_{15} & 0 \\ 0 & 0 & 0 & d_{24} & 0 & d_{26} \\ d_{31} & d_{32} & d_{33} & 0 & d_{35} & 0 \end{pmatrix}.$$

If one neglects absorption and the dispersion of the d coefficients (Kleinman symmetry), the number of independent coefficients drops from 10 to 6, being $d_{15} = d_{31}$, $d_{32} = d_{24}$, $d_{26} = d_{12}$, and $d_{35} = d_{13}$.

The nonlinear optical susceptibilities d_{ip} were determined by a standard Maker-Fringe technique [14, 15] with added suppression of laser beam intensity fluctuations. The fundamental wavelengths were $\lambda = 1542$ nm (first Stokes-line generated in a high pressure Raman cell filled with methane and pumped by a Surelite Nd:YAG laser at $\lambda = 1064$ nm, 7 ns, Q-switched at 2 Hz) and 1907 nm (same laser with the Raman cell filled with high pressure H_2 and Q-switched at 10 Hz). The samples used were an x-plate and a z-plate, from crystals grown at Uzhgorod University (Ukraine), oriented by Laue diffraction (precision ± 6'), polished to optical quality and poled by heating above $T_C = 66°$C and slowly cooling in an applied electric field of 1 kV/cm.

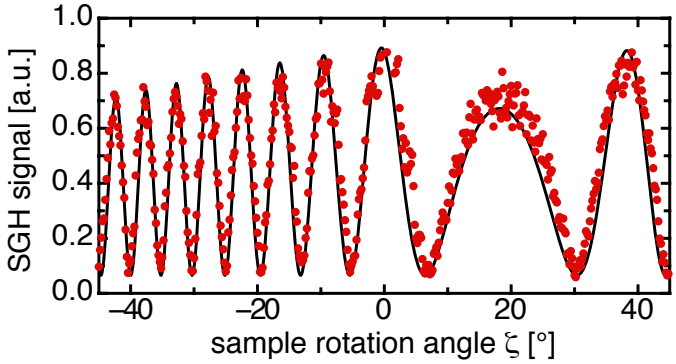

Fig. 1. Maker-Fringe measurement in $Sn_2P_2S_6$ at $\lambda = 1907$ nm and fitted theoretical curve. The sample was a z-plate, which was rotated around its y-axis. The abscissa is the external angle between the fundamental beam (p-polarized) and the z-axis of the crystal. Detected was the p-polarized part of the second harmonic signal, yielding a measurement of d_{11} at the angle $\zeta = 0°$ and a combination of $d_{11}, d_{13}, d_{15}, d_{31}, d_{33}$ and d_{35} for other rotation angles.

#7179 - $15.00 US
Received 15 April 2005; revised 3 May 2005; accepted 5 May 2005

Table 1. All second order nonlinear optical tensor elements d_{ip} of $Sn_2P_2S_6$ at two wavelengths of the fundamental beam. The coefficients are given according to the standard conventions [13] (e. g. $d_{15} = d_{113} = d_{131}$) and a α-quartz reference value of $d^Q_{111} = 0.286\,\mathrm{pm/V}$ at $\lambda = 1542\,\mathrm{nm}$ and $d^Q_{111} = 0.277\,\mathrm{pm/V}$ at $\lambda = 1907\,\mathrm{nm}$ [13].

	d_{ip} at 1542 nm [pm/V]	d_{ip} at 1907 nm [pm/V]
d_{11}	17 ± 1.5	12 ± 1.5
d_{12}	5.2 ± 0.6	2.0 ± 0.3
d_{13}, d_{35}	8 ± 7	6 ± 5
d_{15}, d_{31}	8 ± 10	-1 ± 4
d_{24}	1.3 ± 0.3	1.8 ± 0.5
d_{26}	2.9 ± 0.3	1.7 ± 0.2
d_{32}	6 ± 3	3 ± 2
d_{33}	4 ± 2	4 ± 3

The d coefficients were found by fitting the Maker-Fringe curves and comparing them to the ones of a reference crystal of α-quartz. Fig. 1 shows an example of a Maker-Fringe measurement of $Sn_2P_2S_6$with the corresponding fitted curve. The curve is not symmetrical with respect to the angle $\zeta = 0°$, corresponding to beams perpendicular to the crystal, since the indicatrix is not perpendicular to the Cartesian axes, and therefore the coherence length is minimal at an angle $\zeta \neq 0°$. Nevertheless the theoretical curve describes the experiments nicely. The modified Kleinman symmetries $\delta_{15} = \delta_{31}$ and $\delta_{35} = \delta_{13}$ where used during fitting, while the other Kleinman symmetries where not used, since enough Maker-Fringe curves were available for those coefficients.

The resulting coefficients d_{ip} of $Sn_2P_2S_6$ are shown in Table 1. Note that due to the contribution of several tensor elements in the Maker-Fringe experiments, some of their values could be determined only with a relatively low accuracy. The largest value is the diagonal coefficient

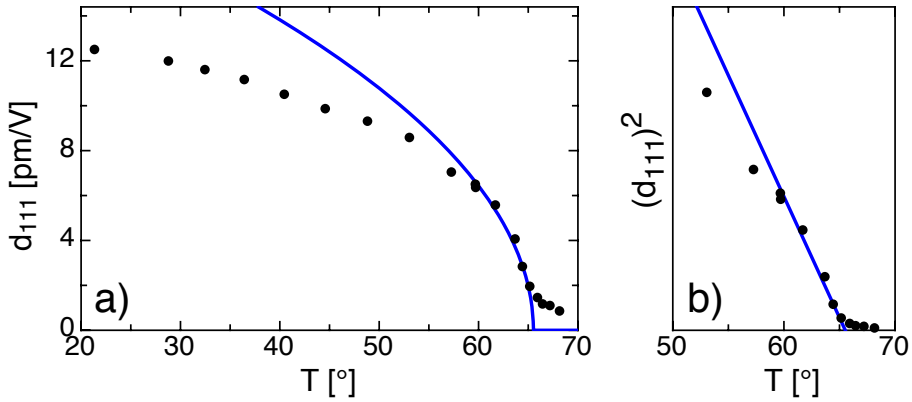

Fig. 2. Temperature dependence of d_{111} at $\lambda = 1907\,\mathrm{nm}$ measured during heating until over the phase transition (a). The solid curve is according to $d_{111} = A(T_C - T)^{1/2}$ with $A = 4.2\,\mathrm{K}^{-1/2}\mathrm{pm/V}$ and $T_C = 65.7°\mathrm{C}$. In (b) the coordinates are chosen so that the dependence of Fig. (a) is linear in the temperature range just below the phase transition.

#7179 - $15.00 US
Received 15 April 2005; revised 3 May 2005; accepted 5 May 2005

$d_{111} = 17 \pm 1.5\,\mathrm{pm/V}$ at $\lambda = 1542\,\mathrm{nm}$ and $d_{111} = 12 \pm 1.5\,\mathrm{pm/V}$ at 1907 nm, which is higher than most of the largest coefficients of standard materials for nonlinear optics. Of special interest is also that $Sn_2P_2S_6$ has very large electro-optical coefficients ($r^T_{111} = 161 \pm 8\,\mathrm{pm/V}$ at $\lambda = 1064\,\mathrm{nm}$ [3]), allowing to combine electro-optical with nonlinear-optical effects.

Fig. 2 shows the temperature dependence of the largest d coefficient at $\lambda = 1907\,\mathrm{nm}$. At this wavelength the influence of temperature on the optical properties is negligible with respect to the change in nonlinear optical properties of second order. The d coefficient is proportional to the electrical polarization [16], which below T_C is given mainly by the acentricity parameter, i.e. the spontaneous polarization P_S. Therefore Fig. 2 represents the temperature dependence of the spontaneous polarization P_S. Close to the phase transition ($T_C - T < 7°\mathrm{C}$) we see the decrease proportional to the square root of $T_C - T$ (Fig. 2(b). The fact that d_{111} does not vanish completely above T_C is explained by thermal fluctuations in the critical region just above the second-order phase transition, induced by residual defects [16].

4. Third harmonic generation

The same laser source as in the case of SHG at $\lambda = 1907\,\mathrm{nm}$ was used for the THG measurements, which were performed using the Maker-Fringe technique in an evacuated chamber ($10^{-2}\,\mathrm{bar}$). As reference we used an α-quartz crystal and the value $\chi^{(3)}_{1111} = 1.99 \cdot 10^{-20}\,\mathrm{m^2/V^2}$ [15].

The measurements showed that $Sn_2P_2S_6$ has very large $\chi^{(3)}$ coefficients:

$$\begin{aligned} \chi^{(3)}_{1111} &= (17 \pm 6) \cdot 10^{-20}\,\mathrm{m^2/V^2} \\ \chi^{(3)}_{2222} &= (9 \pm 3) \cdot 10^{-20}\,\mathrm{m^2/V^2} \end{aligned}$$

corresponding to 850 and 470 times $\chi^{(3)}_{1111}$ of α-quartz and 16 and 8.5 times $\chi^{(3)}_{2222}$ of $KNbO_3$ [15].

5. Phase matching

5.1. Second harmonic generation

In $Sn_2P_2S_6$ phase-matched SHG is possible for a fundamental wavelength in the range between 1680 nm and 8 μm. The whole range is achievable by type I phase matching (incident photons have the same polarisation), while type II phase matching (incident photons are of orthogonal polarisation) is possible for $\lambda > 2324\,\mathrm{nm}$. The upper boundary of 8 μm is given only by the end of the transparency range (see Fig. 3), which is due to phonon-phonon interactions [4].

The refractive indices used for calculating the phase-matching conditions are based on experimental data in the range of $550 - 2300\,\mathrm{nm}$ [6]. This data is precise ($\Delta n = 2 \cdot 10^{-4}$) and fits very well to a two-oscillator Sellmeier model, which was used to extrapolate the refractive indices at longer wavelengths. Nevertheless the precision at larger wavelengths cannot be predicted and could decrease rapidly. For the calculation of d_{eff}, we numerically evaluated (4), taking into account the dispersion of the d_{ijk}, given by Eq. (6). Some analytical expressions for d_{eff} for a biaxial crystal can be found in Refs. 9 and 10.

Fig. 4 shows the phase-matching wavelengths versus the beam direction for type I and type II SHG. The phase-matching loci at the available laser line of $\lambda = 1907\,\mathrm{nm}$ are drawn by the white dashed line. Some experimental points measured at this wavelength are also plotted, demonstrating the accuracy of the calculated phase-matching curve.

In Fig. 5 the regions of internal directions not accessible in crystals cut along the Cartesian x, y, z-axes are indicated by the grey area. For those directions oblique cuts are necessary in order to access the wished internal direction from air. In the following figures this region is

#7179 - $15.00 US Received 15 April 2005; revised 3 May 2005; accepted 5 May 2005

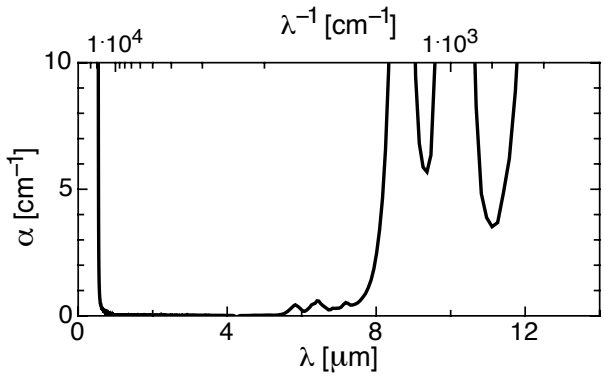

Fig. 3. Absorption constant of $Sn_2P_2S_6$ at room temperature for non-polarized light propagating along the z-axis. It shows the large transparency range extending from $\lambda = 0.53\ \mu$m to $\lambda = 8\ \mu$m. This curve is calculated from measured transmission (by a PE λ9 spectrometer for $\lambda < 1.6\,\mu$m and a PE Paragon FT-IR spectrometer above that wavelength) and taking into account multiple Fresnel reflections.

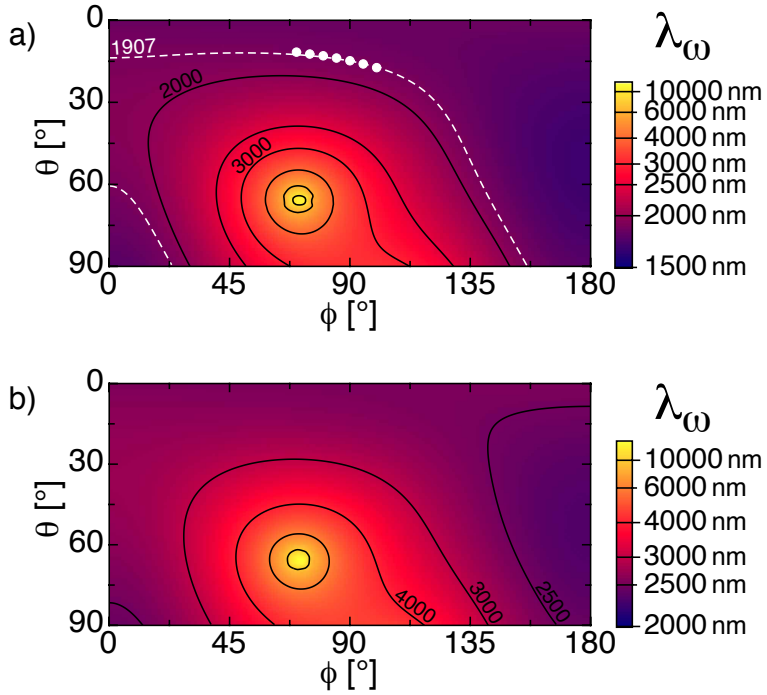

Fig. 4. Directions of phase matching in $Sn_2P_2S_6$ for frequency doubling at room temperature; (a) Type I, (b) Type II. ϕ and θ are the spherical coordinates of the **k** vector in the crystal. Some contour curves are labeled with their corresponding fundamental wavelength in nanometers. The dashed white line corresponds to the predicted phase-matching for the laser line at 1907 nm and the white circles are experimental points.

#7179 - $15.00 US
Received 15 April 2005; revised 3 May 2005; accepted 5 May 2005

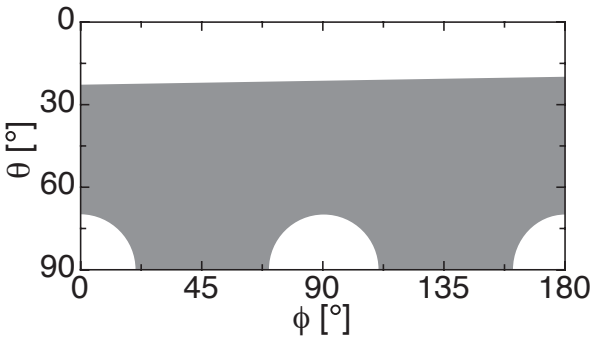

Fig. 5. The grey region indicates the directions that are not accessible from air in crystals cut along the Cartesian x, y, z-axes. This figure was calculated for the wavelengths in Fig. 4(a), but since the dependence on the angles ϕ and θ is much larger than that on the wavelength, it can be assumed valid for every configuration shown in this paper.

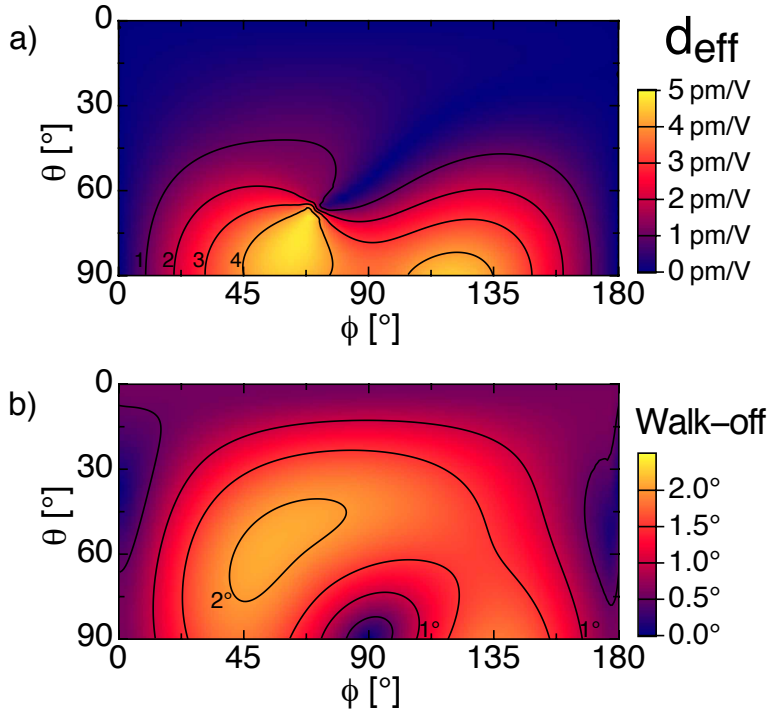

Fig. 6. (a) Effective coefficients and (b) internal walk-off angle for type I phase-matched SHG directions and corresponding wavelengths as in Fig. 4(a).

#7179 - $15.00 US
Received 15 April 2005; revised 3 May 2005; accepted 5 May 2005

either exactly equal or only slightly different than in Fig. 5. All contour plots display the data for the beam directions $\mathbf{k}$ with polar coordinates in the range $\phi \in [0°, 180°]$ and $\theta \in [0°, 90°]$ inside the crystal. In order to get the whole definition range $\phi \in [0°, 360°[$ and $\theta \in [0°, 180°]$ of the spherical coordinates, the following symmetries should be applied

$$\begin{cases} \phi & \rightarrow & 180° - \phi \\ \theta & \rightarrow & 180° - \theta \end{cases} \qquad \text{for } \theta \in [90°, 180°]$$

and

$$\begin{cases} \phi & \rightarrow & 360° - \phi \\ \theta & \rightarrow & \theta \end{cases} \qquad \text{for } \phi \in [180°, 360°[\,.$$

The effective nonlinear optical coefficient is shown in Fig. 6(a) for phase matching of type I. It ranges between 0 and 5 pm/V, with high values of $d_{\text{eff}} > 3$ pm/V for all fundamental wavelengths $\lambda > 1980$ nm. Type II phase matching has large d_{eff} for other wave directions than type I, in particular $d_{\text{eff}} \gtrsim 2$ pm/V for all $\phi > 90°$. Compared to other materials, d_{eff} of $Sn_2P_2S_6$ is similar to the ones of $LiNbO_3$ [17] and KTP [18], and larger than in most other standard materials.

Fig. 6(b) shows the walk-off angle inside the crystal for type I phase matching (PM). For the largest part of directions it lies between 1° and 2°. The corresponding data for type II PM is similar. A special point is given where the walk-off angle is zero, which corresponds to non-critical phase matching. In $Sn_2P_2S_6$ this can occur only for a beam direction parallel to the fixed main axis of the indicatrix, i. e. $\mathbf{k} \parallel y$, corresponding to $(\phi, \theta) = (90°, 90°)$ in the figures. The fundamental wavelength for non-critical PM is $\lambda = 3212.5$ nm for type I and 4536.5 nm for type II. Again, compared to other standard nonlinear optical materials, the walk-off angles are similar to the ones of $LiNbO_3$, and larger than in KTP, but smaller than in BBO.

The figures in this section already give an indication of the possibilities for SFG, since the curves describing phase-matched SFG or OPO collapse in one point with $\lambda_1 = \lambda_2$ for the directions for phase-matched SHG with fundamental wavelength λ_1. The positions of these points were given by the curves in Fig. 4.

5.2. Sum-frequency generation and optical parametric oscillation

In this section we discuss the phase-matching possibilities for SFG or parametric oscillation. The phase-matching condition is given by Eq. (1). In the case of SFG two optical waves at frequencies ω_1 and ω_2 interact to produce a wave at the sum frequency $\omega_3 = \omega_1 + \omega_2$. For parametric oscillation inside a resonant cavity a strong pump wave at frequency ω_3 can produce an idler wave at frequency ω_2 and, through difference frequency generation, a signal wave at frequency $\omega_1 = \omega_3 - \omega_2$. We consider here only configurations in which all wave vectors are collinear. There are two different possibilities for achieving phase matching: (I) The two waves with wavelengths λ_1 and λ_2 share the same polarization, and the sum frequency wave λ_3 is polarized orthogonal to λ_1 and λ_2 or (II) the two waves at the wavelengths λ_1 and λ_2 are polarized orthogonal to each other. In analogy to SHG we call these two cases type I and type II SFG.

In OPO for each beam direction a continuous range of pumping wavelengths can be phase-matched. The phase-matched wavelengths for some propagation directions in the *xy*-plane are given in Fig. 7. With type I PM (left) the curves for λ_1 and λ_2 join smoothly at the wavelength which produces phase-matched second-harmonic radiation. For type II SFG (right) the phase-matching lines intersect where phase-matched SHG is possible. In Fig. 7 the non-critical PM condition ($\mathbf{k} \parallel y$) is shown by a thick line: here with wavelength tuning of $\lambda_3 \in [1000, 1606]$ nm it is possible to get all the wavelengths between 1150 and 8000 nm.

#7179 - $15.00 US
Received 15 April 2005; revised 3 May 2005; accepted 5 May 2005

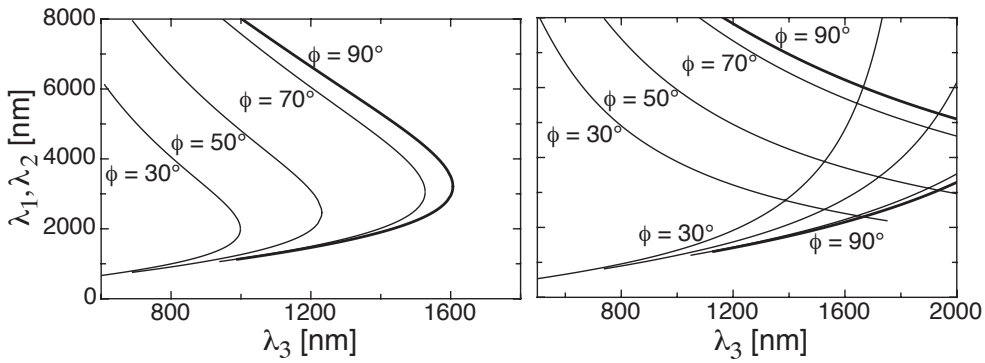

Fig. 7. Angle-tuning for phase-matched sum-frequency generation or optical parametric oscillation. (a) Type I, (b) Type II. Beam propagation is in the *xy*-plane ($\theta = 90°$). λ_3 is the wavelength of the pumping beam, while λ_1 and λ_2 are the wavelengths of the signal and the idler. The bold lines correspond to non-critical phase matching.

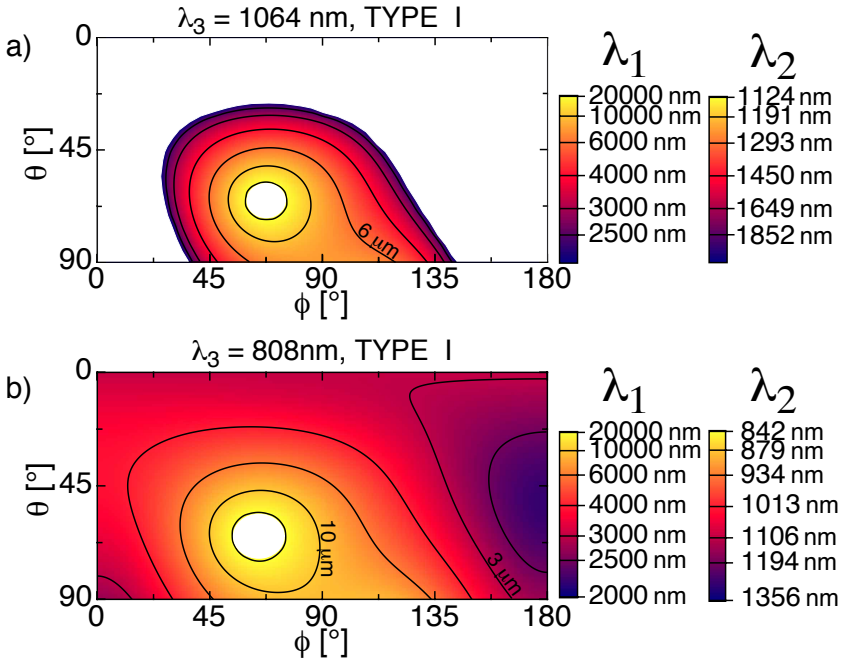

Fig. 8. Phase-matched SFG or OPO of type I for $\lambda_3 = 1064\,\text{nm}$ (a) and $\lambda_3 = 808\,\text{nm}$ (b). The contour lines have constant signal wavelength λ_1 and λ_2, where $\frac{1}{\lambda_1} + \frac{1}{\lambda_2} = \frac{1}{\lambda_3}$. The contour line labels are λ_1 in micrometers. In the outer white region at $\lambda_3 = 1064\,\text{nm}$ no type I PM is possible. In the inner white region one of the phase-matched wavelengths diverges.

#7179 - $15.00 US
Received 15 April 2005; revised 3 May 2005; accepted 5 May 2005

The same result can be achieved by angle-tuning with a fixed pumping wavelength: this can be seen by staying on a vertical line in Fig. 7 and choosing the corresponding value of ϕ for the desired wavelengths λ_1 or λ_2. For the Nd:YAG laser wavelength $\lambda_3 = 1064\,\text{nm}$ this can be also seen in Fig. 8(a), looking at the bottom horizontal line, where $\theta = 90°$. At this wavelength $\lambda_{1,2} \in [1238, 7572]\,\text{nm}$ can be obtained using PM of type I. For the same configuration at the laser diode wavelength of $\lambda_3 = 808\,\text{nm}$, $\lambda_1 > 2747\,\text{nm}$ can be accessed (Fig. 8(b)). Type II PM is also possible, with operating wavelengths similar to type I PM (see Fig. 7(b)). Generally one can access by type II PM the same signal and idler wavelengths as with type I, but the required tuning range of λ_3 is larger and the conversion efficiency lower.

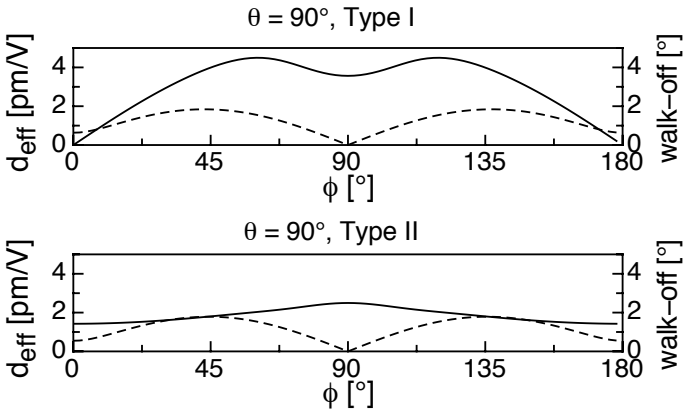

Fig. 9. Effective nonlinear optical coefficient (continuous line) and walk-off angle (dashed line) for phase-matched SFG or OPO with beam propagating in the *xy*-plane ($\theta = 90°$). The dependence of d_{eff} and the walk-off angle on the wavelengths of the interacting beams is weak. The data above is calculated for $\lambda_1 = 2400\,\text{nm}$.

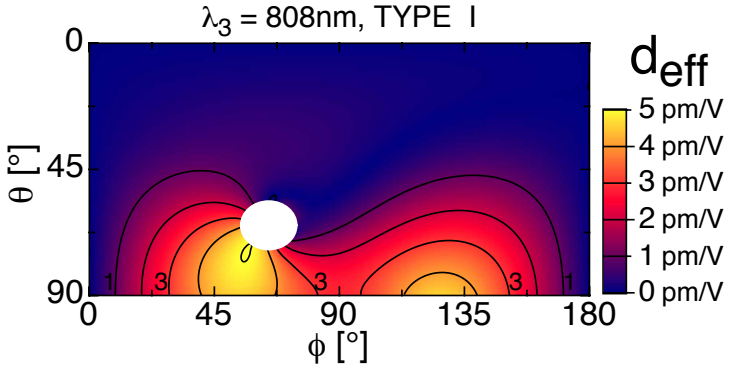

Fig. 10. Effective nonlinear optical coefficient for type I phase-matched SFG or OPO with $\lambda_3 = 808\,\text{nm}$, corresponding to Fig. 8(b). Some contour lines are labeled with their value in pm/V. In the inner white region one of the phase-matched wavelengths diverges.

For the efficiency of these frequency conversions refer to Fig. 9, where d_{eff} and the walk-off angle are displayed for $\mathbf{k}$ in the *xy*-plane ($\theta = 90°$). These two parameters depend very little on the interacting wavelengths, and $d_{\text{eff}} > 3\,\text{pm/V}$ for type I PM in the range $\phi = 30° \ldots 150°$,

#7179 - $15.00 US
Received 15 April 2005; revised 3 May 2005; accepted 5 May 2005

while for type II d_{eff} is around 2 pm/V in the whole range of ϕ. The largest contributions to d_{eff} around the non-critical PM direction ($\theta = \phi = 90^\circ$) are given by d_{111} and d_{133}, with these two contributions having the same sign for type I and different one for type II PM. With ϕ moving away from 90°, the term with d_{133} becomes dominant for type I, while for type II many terms roughly balance each other. The efficiency for general beam directions is shown in Fig. 10 for $\lambda_3 = 808$ nm. It is highest for θ near 90°, and remains large as long as the internal angle between **k** and the *xy*-plane does not exceed $20 - 30^\circ$. The same figure at $\lambda_3 = 1064$ nm is very similar. By pumping at that wavelength, with a crystal cut perpendicularly to ($\theta = 90^\circ, \phi = 45^\circ$), one can for example access all wavelengths $\lambda_{1,2} > 1200$ nm by type I phase-matched angle-tuning and with $d_{\text{eff}} \approx 4$ pm/V.

6. Conclusions

The nonlinear optical coefficients of ferroelectric $Sn_2P_2S_6$ were measured for $\lambda = 1542$ nm and 1907 nm at room temperature. The largest coefficients at these wavelengths are $d_{111} = 17 \pm 1.5$ pm/V and $d_{111} = 12 \pm 1.5$ pm/V, respectively. Third order subsceptibilities $\chi^{(3)}_{1111} = (17 \pm 6) \cdot 10^{-20}\,\text{m}^2/\text{V}^2$ and $\chi^{(3)}_{2222} = (9 \pm 3) \cdot 10^{-20}\,\text{m}^2/\text{V}^2$ were measured at $\lambda = 1907$ nm. The temperature dependence of d_{111} confirmed the temperature dependence of the spontaneous polarization within a temperature range of about 7°C below the Curie temperature $T_C \approx 66$°C.

Based on the new refractive-index data for $Sn_2P_2S_6$, we have analyzed various nonlinear optical second-order interactions. Phase-matching configurations for various wavelengths and beam propagation directions have been studied. The principal polarization directions, walk-off angles, acceptance angles, and effective nonlinear-optical coefficients have been calculated numerically for arbitrary beam propagation directions in this biaxial crystal. Phase matching has been found to be possible in a large variety of configurations. For example type I phase-matched optical parametric generation from 1.2 to 8 μm with $d_{\text{eff}} \approx 4$ pm/V is possible using a Nd:Yag pumping laser and similarly from 2.3 to 8 μm using a laser at 808 nm.

The advantages of this crystal are its large transparency range extending from 0.53 to 8 μm, the possibility for phase matching in the whole transparent range, the good nonlinear efficiency at phase matching, the very large electro-optical coefficients and the absence of hygroscopicity. The walk-off angle ranges between 0 and 2°, similarly to $LiNbO_3$ but larger than in KTP. Damage threshold studies will be required to fully assess the potentiality of this crystal for high-power near infrared frequency conversion.

Acknowledgments

We thank A. Grabar and Y. Vysochanskii for supplying the crystals and the Swiss National Foundation for the financial support (NF 2-777416-04).

#7179 - $15.00 US Received 15 April 2005; revised 3 May 2005; accepted 5 May 2005